




Advanced Carbon Based Materials for Fabrications of Sodium Ion Hybrid Capacitors with High Electrochemical Performance



Jianke LI,^{a,c,†} Wenjie LIANG,^{a,†} Xincheng MIAO,^{a,c,*} Beibei HAN,^{b,e} Guiying XU,^{a,*} Kun WANG,^{a,d,*} Baigang AN,^a Dongying JU,^{b,f} Maorong CHAI,^b and Weimin ZHOU^{a,*}

^a Key Laboratory of Energy Materials and Electrochemistry Research Liaoning Province, University of Science and Technology Liaoning, No. 189 Qianshan Middle Road, Lishan District, Anshan City, Liaoning Province, Anshan 114051, China

^b Advanced Science Research Laboratory, Saitama Institute of Technology, 1690 Fusaiji, Fukaya, Japan

^c School of Materials and Metallurgy, University of Science and Technology Liaoning, No. 189 Qianshan Middle Road, Lishan District, Anshan City, Liaoning Province, Anshan 114051, China

^d Sinosteel Anshan Research Institute of Thermo-Energy Co., Ltd., No. 301 Anqian Road, High-tech Zone, Anshan City, Liaoning Province, Anshan 114051, China

^e Key Laboratory of Advanced Fuel Cells and Electrolyzers Technology of Zhejiang Province, Ningbo Institute of Materials Technology and Engineering, Chinese Academy of Sciences, Ningbo, No. 1219 Zhongguan West Road, Zhejiang 315201, China

^f Hainan University, 58 Renmin Avenue, Haikou 570228, China

* Corresponding authors: asust_msn@163.com (X. M.), xuguiying751107@163.com (G. X.), ustl15542731203@163.com (K. W.), aszhou15242870697@163.com (W. Z.)

ABSTRACT

Herein, the novel sodium ion hybrid capacitors (SIHCs) are successfully and facilely fabricated by utilizing the same carbon resource of magnesium citrate. Namely, the carbons which are fabricated by immediate carbonizations of magnesium citrate are used as positive electrodes, and N, S-doped carbons prepared by co-carbonizations of magnesium citrate with ammonium persulfate are determined as negative electrodes. The detailed electrochemical evaluations demonstrate that fabricated SIHCs possess tremendous Na⁺ storage performance. For instance, the fabricated SIHC(1//1) shows an energy density of 100.8 Wh Kg⁻¹ at a power density of 136.8 W Kg⁻¹, when current density was 0.1 A g⁻¹. Furthermore, when the current density was set at 5.0 A g⁻¹, this SIHC(1//1) also exhibits a power density of 12957.6 W Kg⁻¹ at an energy density of 46.9 Wh Kg⁻¹. These results reveal that SIHC(1//1) has the powerful competitiveness in high energy and power-required electricity storage applications.

© The Author(s) 2023. Published by ECSJ. This is an open access article distributed under the terms of the Creative Commons Attribution 4.0 License (CC BY, <http://creativecommons.org/licenses/by/4.0/>), which permits unrestricted reuse of the work in any medium provided the original work is properly cited. [DOI: [10.5796/electrochemistry.23-00012](https://doi.org/10.5796/electrochemistry.23-00012)].



Keywords : Hard Carbons, Sodium Ion Hybrid Capacitors (SIHCs), Magnesium Citrate, N, S-doped Carbons

1. Introduction

More recently, developing the energy storage systems (ESSs) has become one of the urgent tasks for the countries working to build a new energy sector that rationally and efficiently utilizes the solar energy, wind energy and other renewable energies. Admittedly, the lithium ion batteries (LIBs) are a good selection for ESSs, however, the safeties in utilization and resource of LIBs lead the numerous scientific research workers to search alternatives. The sodium ion batteries (SIBs) for ESSs have drawn a lot of attention because the sodium possesses more remarkable resource superiorities than the lithium.¹⁻⁷ Nevertheless, the storage capacity of SIBs cannot satisfy the demands of energy storage devices which simultaneously couple the high energy densities and power densities. Facing the demands above, the sodium ion hybrid capacitors (SIHCs) are expected to be a pivotal alternative because they have virtues of high energy densities and power densities.⁸⁻¹⁶ It is acknowledged that the designs and fabrications of electrode materials are very critical for developing the electrochemical performance of SIHCs.

So far, several anode materials and the typical activated carbon (AC) cathode have been applied in SIHCs.¹⁷ Among the materials

fabricating the electrodes of SIHCs, the carbon materials such as hard and soft carbons become the preferred materials gradually due to their extensive resources, stable structure, good electrical conductivity, low price, and adjustable structure. Especially, hard carbons are considered as a preferential choice to fabricate the SIHCs because they are capable to have bigger inter lamellar space and specific surface area than the others.^{18,19}

As is known to all, the appropriateness between the positive and negative electrodes is a critical factor to fabricate the SIHCs having the excellent electrochemical performance.¹⁷⁻²⁵ It is interestingly reported that the carbon materials which are simultaneously used as positive and negative materials can realize the subject that how to obtain the better appropriateness between the positive and negative electrodes.⁸ In addition, Yang et al., have pointed out that the similar material systems are beneficial to solve the structural stabilities in SIHCs.^{17,26,27} Therefore, the aforementioned descriptions lead us to consider that if the materials fabricating the SIHCs are the same hard carbon materials, the pivotal fabrication factors such as appropriateness and structural stability will be addressed well.

Specifically, during the fabrications of electrode materials, it is worth noting that the structures of positive electrodes are needed to have a high specific area and porous structures.¹⁹ In general, the method using the template is an effective way to prepare the carbons with complex porous structures. In recent years, plenty of hard templates such as mesoporous silica, SiO₂ spheres, MgO and

[†]These authors (Jianke LI and Wenjie LIANG) contributed equally to the work.

[§]ECSJ Active Member
W. Zhou  orcid.org/0000-0001-6703-465X

montmorillonite are developed and utilized in cases to fabricate materials with complex porous structures.^{28–31} In contrast to the templates such as mesoporous silica, SiO₂ spheres and montmorillonite, the MgO template possesses the advantages such as cheapness, chemical stability and high thermal stability, which make it exhibit a better application prospect than the others.³⁰ Mansour observed that the mixture products of carbon and MgO appeared when carrying out the pyrolysis of magnesium citrate 14-hydrate.³² Subsequently, the porous carbon materials were fabricated by co-carbonization using magnesium citrate as a MgO template and poly(vinyl alcohol) (PVA).³⁰ These previous studies lead us to want to obtain positive electrodes through the direct carbonization of magnesium citrate.

Besides, the excellent reaction kinetics is an another important point to promote the Na⁺ storage capacity of carbon materials.^{18,21–23} Doping the N or S elements is an effective way to improve the electrolyte infiltration and expand the distances between the carbon layers, leading to the improvement of reaction kinetics.^{21,25} In our case, the N and S doped processes are realized by co-carbonizations of magnesium citrate with ammonium persulfate, and the N, S-doped carbons are used as negative electrodes of SIHCs. In this case, it is impressively observed that the intermediate of (NH)₂Mg₂(SO₄)₃ clearly produced in co-carbonizations, and it can immediately be changed to the MgSO₄, with conducting the N-doped process. Meanwhile, the produced MgSO₄ can fortunately realize the S-doping very well, because the MgSO₄ is able to prevent the loss of S elements in co-carbonizations.

After the SIHCs had been assembled by utilizing the fabricated positive and negative electrodes with different mass ratios, their electrochemical performance was evaluated in detail. For instance, when a mass ratio is set as 1 : 1, the assembled SIHC(1//1) manifests a higher energy density and power density than other SIHCs constructed by different mass ratios. As a result, the electrochemical evaluations indicate that using the same carbon resource of magnesium citrate is a feasible and effective way to fabricate electrodes of SIHCs having high electrochemical performance. The formations of MgO template in the direct carbonization of magnesium citrate and MgSO₄ dopant in co-carbonization of magnesium citrate with ammonium persulfate are the key components for fabricating the electrodes of SIHCs having the significantly high electrochemical performance. That is also our research feature of electrode fabrications for SIHCs.

2. Experimental Section

2.1 Chemicals

The magnesium citrate (purity ≥ 99.7 %) and ammonium persulfate (purity ≥ 99.5 %) were purchased from Sinopharm Chemical Reagent Co., Ltd, P.R. China. All chemicals were used without any further purification.

2.2 Fabrication of magnesium citrate based porous carbon materials

Firstly, after adding the magnesium citrate (MC) (5 g) to a quartz boat, the quartz boat was placed in a carbonization furnace. The temperatures of carbonization furnace were respectively increased to 650 °C, 750 °C and 850 °C at a heating rate of 3 °C/min, and these temperatures were held at 650 °C, 750 °C and 850 °C for 1 h. After cooling down to room temperature, the obtained carbon materials were washed by HCl (1M) several times. And then they were filtered, the obtained solids were washed with deionized water until the pH of the washed water became neutral. Finally, the filtered products were dried for 12 h at 100 °C in a vacuum drying oven. According to the different carbonization temperatures, the final products were respectively named as MCC-650, MCC-750 and MCC-850.

2.3 Fabrication of N, S doped carbon materials

In accordance with a mass ratio of 5 : 1, the MC (5 g) and ammonium persulfate (1 g) were added to a porcelain ark, and then this porcelain ark was placed in a carbonization furnace, in which the temperatures were respectively increased to the 650 °C, 750 °C and 850 °C with a heating rate of 3 °C/min. These temperatures were maintained at 650 °C, 750 °C and 850 °C for 1 h. Similarly, the prepared solids were also treated with HCl (1M) several times, and then they were washed with deionized water until the pH values of scrubbing solutions became 7. The obtained carbon materials were finally placed in a vacuum drying oven and dried for 12 h at 100 °C. Likewise, the resulting materials were designated as NSMCC-650, NSMCC-750 and NSMCC-850, respectively.

2.4 Characterization

The measurements of X-ray diffraction (XRD) used an X'pert Powder instrument from PANalytical. The X-ray photoelectron spectroscopy (XPS) measurements were carried out on a K-Alpha instrument from Thermo Fisher Scientific, USA. Nitrogen adsorption and desorption isotherms were measured by a Quadrasorb-iQ surface analyzer which was purchased from Quantachrome Instruments, USA. Specific surface areas were determined in detail, according to the Brunauer-Emmett-Teller (BET) method. The pore size distribution was assessed by a density functional theory (DFT) model for slit pores. Morphologies were evaluated by scanning electron microscopy (SEM) using an instrument produced by Carl Zeiss AG, Germany).

2.5 Electrochemical measurements

The prepared MCC or NSMCC materials, acetylene black and polyvinylidene fluoride (PVDF) were ground in an agate mortar with a mass ratio of 8 : 1 : 1 until the mixture was uniform. After adding an appropriate amount of N-methyl-2-pyrrolidone (NMP) into the above mixtures, the mixtures were mixed homogeneously. The obtained slurries were evenly coated onto the collectors (aluminum foil for the positive electrode and copper foil for the negative electrode), and collectors were placed in a vacuum drying oven for 12 h at 120 °C. After cooling to room temperature, they were cut into electrodes with a diameter of 11 mm. Hereto, the positive and negative electrodes were respectively prepared by using the MCC and NSMCC materials. The mass loadings of MCC and NSMCC electrodes were controlled at 1.68 mg/cm² and 1.26 mg/cm², respectively.

In a glove box filled with argon, the CR2032 sodium button half cells were assembled by the above-mentioned positive and negative electrodes, metal sodium sheets ($\phi = 15$ mm), glass fiber diaphragms (GF/D) and electrolyte of 1M NaClO₄ in ethylene carbonate (EC)/dimethyl carbonate (DMC) (1 : 1 by volume) with 5 vol% fluoroethylene carbonates (FEC). After the electrochemical performance of half cells had been investigated in detail, the suitable materials for fabricating the electrodes of SIHCs were decided.

The electrodes were conducted pretreatments before assembling of sodium ion hybrid capacitors (SIHCs). Firstly, the half cells were assembled by using the NSMCC materials as anode, and carried out charge-discharge 5 cycles at 0.1 A/g until discharged to 0.01 V, in order to form the stable SEI on the surface of NSMCC materials. Meanwhile, the MCC materials as positive electrode were also used to assemble half cells, and then they were performed charge-discharge 5 cycles until charged to 4.2 V so as to fill the electrodes with ClO₄⁻.^{33,34}

Thereafter, the above half-batteries were disassembled, and the electrodes were removed to fabricate electrodes of SIHCs. The negative and positive materials were respectively coated on the copper foil and aluminum foil, in order to fabricate SIHCs.²⁵ The electrolyte and diaphragm were the same as those used above.

The cut-off voltages of charge and discharge were respectively set at 2.50–4.20 V (positive electrode)/0.01–3.00 V (negative electrode)/0–4.00 V (SIHC). The cyclic voltammetry scanning voltage ranges are 2.50–4.20 V (positive electrode)/0.01–3.00 V (negative electrode)/0–4 V (SIHC). The potential mentioned in this study is Na^+/Na redox potential.³⁵

LAND CT-2100A battery testing system was used to test the electrochemical performance of the buckle battery. Cyclic voltammetry and electrochemical impedance spectroscopy (over a frequency range of 100 kHz–0.01 Hz and the amplitude was 5 mV) were tested by CHI660E electrochemical workstation (ChenHua, Shanghai, China).

3. Results and Discussion

3.1 Structures and morphology characteristics of MCC and NSMCC materials

The origin of the names of MCC and NSMCC are introduced in Experimental Section. The morphologies of MCC and NSMCC materials were firstly characterized by the SEM measurements (Fig. 1). It was clearly observed that MCC materials possessed smaller particle sizes than the NSMCC materials, and NSMCC materials owned relatively large pore structures. The different morphologies and structures between the two materials indicate that MCC and NSMCC materials undergo different carbonization processes (Figs. 1a–1f). In the Figs. S1a–S1c, the SEM-EDS images of NSMCC materials indicated that N and S elements are uniformly distributed in the NSMCC materials.

To further inquire into the porous structures and specific surface areas of MCC and NSMCC materials, the BET measurements were conducted in detail (Fig. S2). The specific surface areas of MCC materials were calculated at $1529.1 \text{ m}^2 \text{ g}^{-1}$, $1210.2 \text{ m}^2 \text{ g}^{-1}$ and $1169.5 \text{ m}^2 \text{ g}^{-1}$, revealing specific surface areas diminished with increasing carbonization temperatures. On the contrary, the specific surface areas of NSMCC materials were $745.8 \text{ m}^2 \text{ g}^{-1}$, $917.3 \text{ m}^2 \text{ g}^{-1}$ and $1074.6 \text{ m}^2 \text{ g}^{-1}$, respectively, showing an increased tendency with increasing carbonization temperatures. Compared to the MCC materials, the different tendencies of specific surface areas also indicate that the NSMCC materials owned a different carbonization process from the MCC materials. In addition, the porous structures of MCC and NSMCC materials were detailedly evaluated by using the DFT method. After calculations, the pore diameters of MCC-650 (1.4 and 3.7 nm), MCC-750 (1.1 nm, 3.6 nm and 8.2 nm) and MCC-850 (1.4 nm, 4.5 nm and 7.4 nm) were verified respectively. In contrast, the pore diameters of NSMCC-650 (1.4 nm, 3.3 nm and

5.6 nm), NSMCC-750 (1.4 nm, 3.3 nm, 5.4 nm, 7.8 nm and 11 nm) and NSMCC-850 (1.4 nm, 3.6 nm, 7.8 nm and 10.7 nm) were also clearly observed, indicating that porous structures of NSMCC materials are larger than the MCC materials (Fig. S2 and Table S1). Nevertheless, compared to the NSMCC materials, the MCC materials manifested a bigger total volume than that of NSMCC materials, conjecturing that the porous distribution status of MCC materials are extremely better than that of NSMCC materials. Therefore, a reason that MCC-750 possesses a bigger specific surface area and total volume than other fabricated materials can be ascribed to its numerous microporous structures (Table S1).

In order to survey the formation processes of porous structures of MCC and NSMCC materials, the structures of materials without washing with HCl and water were analyzed in detail. In the carbonization cases of MCC materials, it was aware that the Mg^{2+} started to change into the MgO compounds, when the carbonization temperature was increased to 450 °C. After the carbonization temperature had been increased to 850 °C, it was found that the intensity of MgO became strong exceedingly, indicating that Mg^{2+} entirely changed to the MgO in MCC materials before acid pickling processes (Fig. 2a). Besides, it was different from the MCC fabrication cases, the $(\text{NH})_2\text{Mg}_2(\text{SO}_4)_3$ appeared in the NSMCC materials when the carbonization temperatures were set at a range of 250–350 °C (Fig. 2b).

Furthermore, the $(\text{NH})_2\text{Mg}_2(\text{SO}_4)_3$ changed to the MgSO_4 at 450–650 °C, demonstrating that the N-doping process was mainly conducted in this temperature range. Additionally, it was distinct that the MgSO_4 completely disappeared at 750–850 °C, revealing that MgSO_4 changed to the MgO, and S-doping was also performed at the same time. It is noteworthy that the formation of MgSO_4 is able to diminish the loss of S element in co-carbonization processes, causing the S-doping amount to increase remarkably (Fig. 2b).

After the obtained MCC and NSMCC materials had been washed by the HCl and H_2O , their structures were also evaluated by the XRD measurements (Fig. S3). As shown in Fig. S3, the broad peaks of 23° corresponding to the (002) plane slightly shifted to a larger angle, indicating that the degree of graphitization raised with increasing the carbonization temperature in the MCC fabrication cases. By contrast, the observations that (002) peaks shift to the lower value are suggestive of that structures of NSMCC materials became disorder with increasing the carbonization temperature.³⁶

Similar to the report by Liu and Luo et al., the R values were used to evaluate the disorder degree of MCC and NSMCC materials (Fig. S4a).^{37,38} It is well-known that low R values can reveal that materials possess significant disorder structures. The R values of

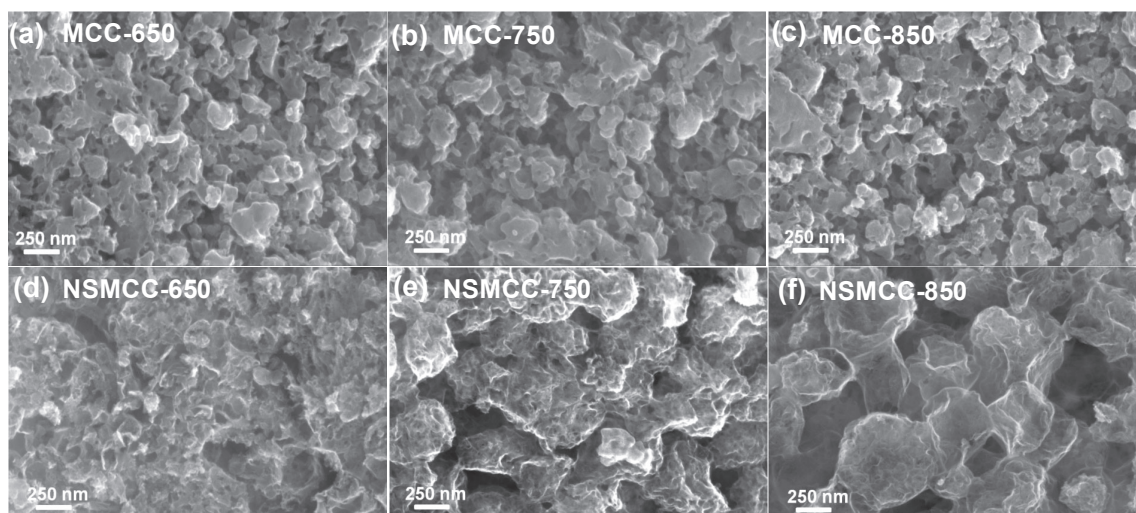


Figure 1. SEM morphologies of MCC-650 (a), MCC-750 (b), MCC-850 (c), NSMCC-650 (d), NSMCC-750 (e) and NSMCC-850 (f).

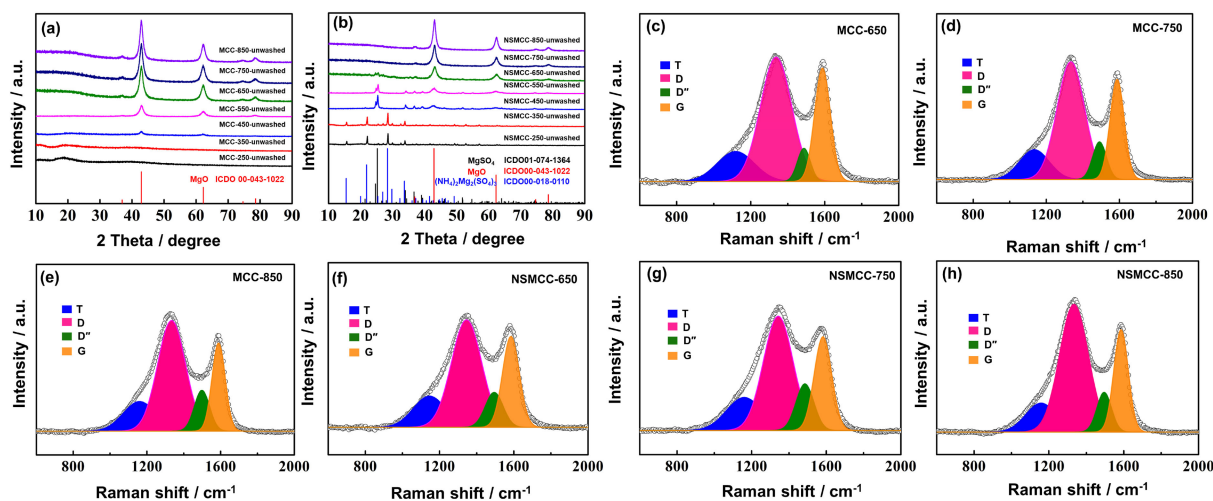


Figure 2. XRD results of MCC (a) and NSMCC carbon materials without the acid pickling treatments (b). Fitted Raman spectra of MCC materials (c–e) and NSMCC materials (f–h). Among them, T band is the stretching vibrations of C–C and C=C or sp^2 - sp^3 bonds in polyene-like structures. D band refers to a breakdown of symmetry for small graphitic crystallites carbon atoms at the edge of graphene layers. D' band can be attributed to distortions of the inner symmetry in aromatic rings. G band corresponds to the planar motion of sp^2 -hybridized carbon atoms in an ideal graphene layer.

MCC materials show an increased tendency, indicating that the graphitization degrees of MCC increase gradually, with increasing the carbonization temperatures (Table S2 and Fig. S4b). On the other hand, the trend of R values of NSMCC materials is initially going upward and then downward, which reveals that NSMCC-750 possesses more disorder structures than the NSMCC-650 and NSMCC-850 materials (Table S2 and Fig. S4b). Associated with the analyses upon the structures of NSMCC without washing with HCl and H₂O, it is considerable that suitable doping dosages of N and S elements are the probable reason leading to the degree decrease of graphitization of NSMCC-750.²⁹

The conversions of interlayer spaces were investigated by the peak fitting of XRD charts (Fig. S5). After calculations, the interlayer spaces of MCC-650, MCC-750 and MCC-850 were calculated at 0.365 nm, 0.364 nm and 0.362 nm, respectively, indicating that the interlayer spaces decreased with increasing the carbonization temperatures. Besides, the NSMCC-750 exhibited a bigger interlayer space (0.372 nm) than the NSMCC-650 (0.367 nm) and NSMCC-850 (0.366 nm), which was naturally attributed to a reason that plenty of N and S elements were doped in the NSMCC-750 materials (Fig. S5 and Table S3).

Raman measurements were also performed so as to analyze the structural conversions, with increasing the carbonization temperature (Figs. 2c–2h). In general, the D peak attributing to the defects on the graphite edge and the G peak from the sp^2 structures on carbon sheets were observed at 1355 cm^{-1} and 1600 cm^{-1} , respectively. The intensity ratios (I_D/I_G) of D and G peaks can reflect the disorder degree and surface defects. As shown in Table S3, it was aware that the I_D/I_G values showed an obvious upward tendency with increasing the carbonization temperatures, indicating that the degree of graphitization of MCC materials increased gradually. On the other hand, it was different from the MCC materials, the NSMCC-750 showed a smaller I_D/I_G value than the NSMCC-650 and NSMCC-850, suggesting that the NSMCC-750 owned a smaller degree of graphitization than that of the NSMCC-650 and NSMCC-850. As a consequence, the Raman measurements are perfectly consistent with the XRD analyses.

XPS measurements were used to evaluate the chemical states of MCC and NSMCC materials. As shown in Fig. 3a, it can be seen that the peaks of C and O elements in MCC and NSMCC materials were observed at 284.8 eV and 531.5 eV, respectively. Meanwhile,

the peaks of N and S in NSMCC materials were observed at 399.7 eV (N 1s), 228 eV (S 2s) and 163.2 eV (S 2p), respectively. Figure 3b exhibited that S contents in NSMCC-650, NSMCC-750 and NSMCC-850 were the 2.48 %, 5.11 % and 4.98 %, respectively (Table S4a). Meanwhile, the types of functional groups containing S were verified by the fitting of S 2p (Figs. 3c–3e). The peaks of 164.0 eV, 165.1 eV and 167.7 eV corresponding to the S 2p_{3/2} (–C–S–C–), S 2p_{1/2} (–C–S–C–) and –S=O, –S–O were verified respectively.³⁶ Additionally, the content of –C–S–C– showed a first upward and then downward tendency, and contents of –S=O, –S–O still increased, with raising the carbonization temperatures. These changes in contents of groups containing S elements are indicative of that the –C–S–C– group partly changed to the –S=O and –S–O groups.

Similar to S contents, the N contents also showed the first increasing and then decreasing tendency. A possible explanation is attributed to that the N elements partially lost in the carbonization at the temperature of 850 °C. The varieties of N elements were verified by the fitting of N 1s. As per Figs. 3f–3h, the peaks of N-6, N-5 and N-Q were observed at 398.6 eV, 400.8 eV and 402.6 eV, respectively.³⁹ As shown in Table S4b, it was obvious that NSMCC-750 possessed higher contents of N-6, N-5 and N-Q than that in other NSMCC materials. On the basis of the full analyses of structures and chemical states of MC and NSMC materials, the selections of electrodes of SIHCs were conducted comprehensively.

3.2 The selection of anode materials of SIHCs

Likewise, the anode deciding rule is generally dependent upon the storage capacity of materials at a potential range of 0.01–3 V.³⁹ The electrochemical properties of MC and NSMC materials were investigated synthetically by analyzing several aspects of cycling performance, rate performance, cyclic voltammetry, and dynamic performance.⁴⁰

In the charge-discharge processes, it was observed that the MCC-650, MCC-750 and MCC-850 showed the initial coulomb efficiency (ICE) at 14.7 %, 11.2 % and 8.8 %, respectively, and the ICE of NSMCC-650, NSMCC-750 and NSMCC-850 were 22.99 %, 20.71 % and 14.19 %, respectively (Fig. S6). The reason that MCC-650, MCC-750 and MCC-850 possessed smaller ICE than the NSMCC-650, NSMCC-750 and NSMCC-850 was generally attributed to that the MCC materials owned larger specific surface

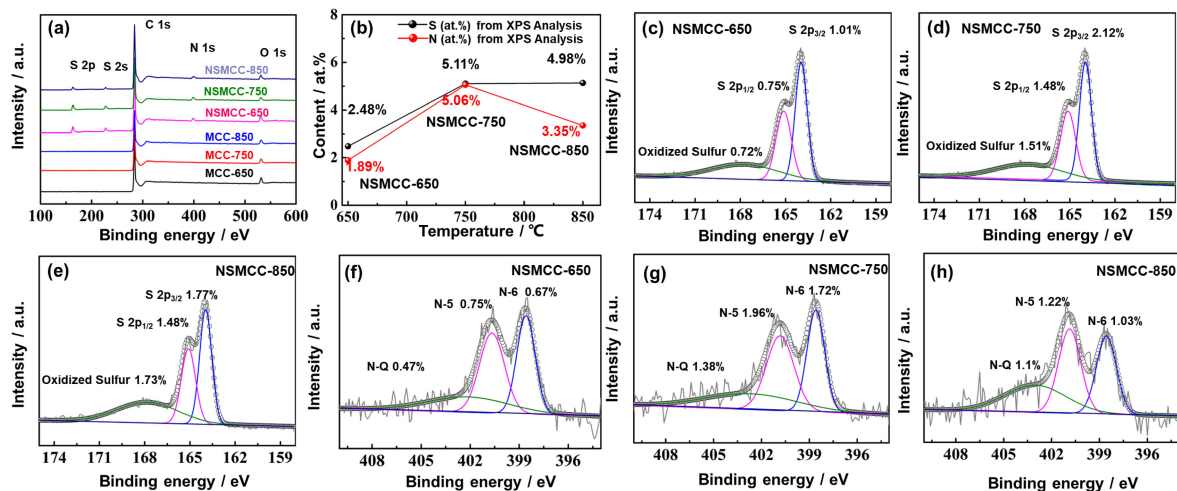


Figure 3. XPS survey spectra of MCC and NSMCC materials (a). S and N contents in NSMCC materials from XPS analysis (b). High-resolution spectra with peak fittings of S 2p for NSMCC materials (c–e). High-resolution spectra with peak fittings of N 1s for NSMCC materials (f–h).

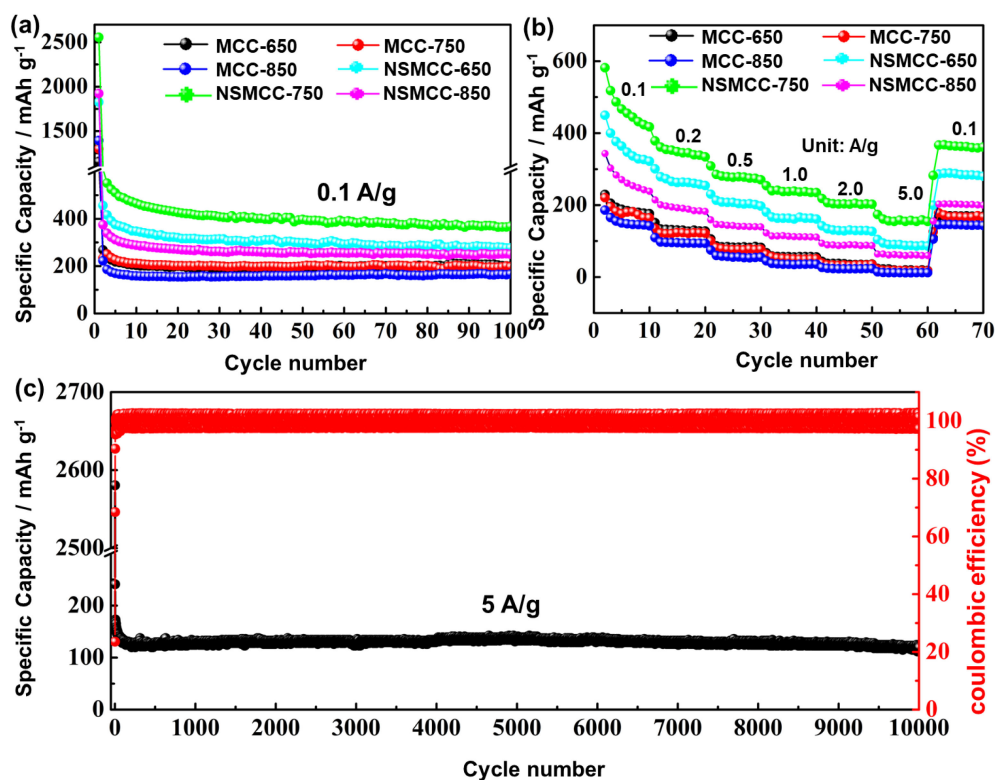


Figure 4. (a) Cycling performance of MCC and NSMCC materials. (b) Rate performance of MCC and NSMCC materials. (c) Long cycling performance of NSMCC-750 materials at big current densities of 5 A g^{-1} .

area than that of NSMCC materials, leading to the larger irreversible capacity relating to formations of SEI on the surface of MCC materials (Table S1).

As shown in Fig. 4a, the NSMCC-750 showed more tremendous storage capacity than other MCC and NSMCC materials at 0.01–3 V. For instance, the Na^+ storage capacity of NSMCC-750 was 581.5 mAh g^{-1} after 100 cycles at 0.1 A g^{-1} . Furthermore, the NSMCC-750 also showed excellent cycling stability at a big current density. As an example, when the current density was adjusted to 5.0 A g^{-1} , the storage capacity of NSMCC-750 still has 119.8 mAh g^{-1} over 10000 cycles (Fig. 4c). The comparisons of the rate performance reveal that the NSMCC-750 possesses a more

excellent electrochemical performance (Fig. 4b). Consequently, NSMCC-750 can be selected as anode materials from the premise that the high storage capacity mainly is in a range of 0.01–3 V. Moreover, in order to fully understand the reason why the NSMCC-750 material possesses the higher storage capacity, other electrochemical evaluations were conducted.

Electrochemical impedance spectroscopy (EIS) tests of MCC and NSMCC electrode materials were further performed (Fig. 5). After fitting and calculating, the R_3 resistance values of MCC-650 (684.1Ω), MCC-750 (1163.0Ω), MCC-850 (1386.0Ω), NSMCC-650 (184.5Ω), NSMCC-750 (144.4Ω) and NSMCC-850 (228.2Ω) were obtained respectively (Figs. 5a and 5c), indicating that the

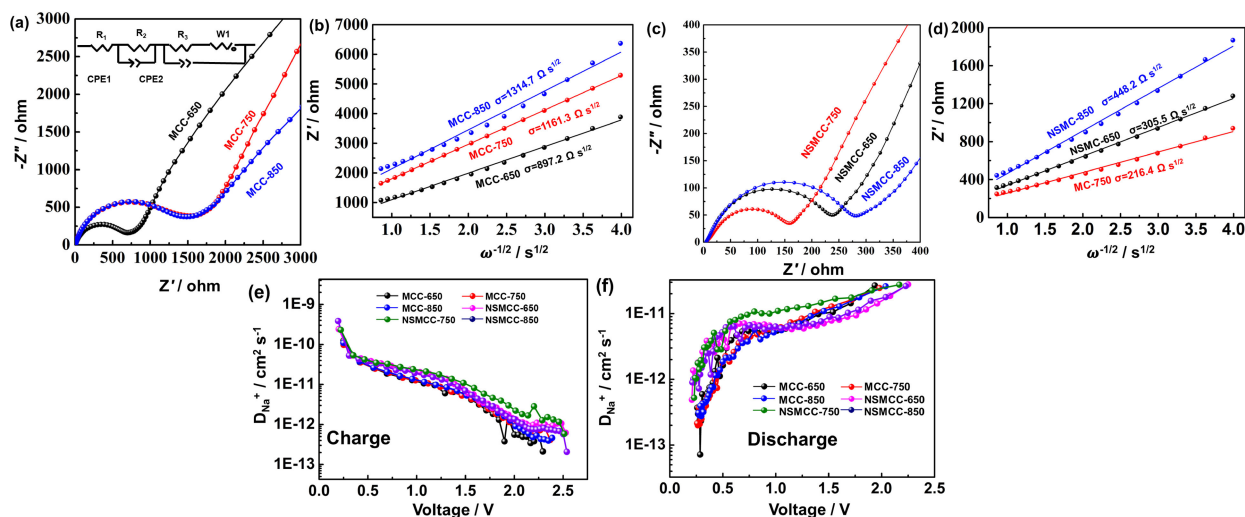


Figure 5. Nyquist plot results (a, c) and illustrations of relationships between Z' and $\omega^{-1/2}$ in the low-frequency region (b, d). Thereinto, R_1 is the total resistance of the electrolyte, separator, and electrical contacts; R_2 and R_3 are the Na^+ migration resistance through the SEI film and charge-transfer resistance, respectively; W_1 is the Warburg impedance connected with the Na^+ diffusion process; CPE1 and CPE2 represent the double layer resistance. Relationships between voltage and Na^+ diffusion coefficient during the charge (e) and discharge states (f).

NSMCC materials possessed the more excellent charge-transfer abilities than the MCC materials, which was attributed to that doping the N and S in structures of NSMCC materials improved the infiltration of electrolyte (Tables S4a–S4b). Furthermore, among the NSMCC materials, the NSMCC-750 apparently owned more tremendous conductivities than other NSMCC materials (Table S5).

The dynamic evaluations were further characterized by the σ value of the Warburg coefficient (Figs. 5b and 5d). The σ values could be obtained by measurements of the Randles plot plotting of Z' with $\omega^{-1/2}$ ($\omega = 2\pi f$) for a low-frequency. The large value of σ is able to reflect the poor ion diffusion performance. As a result, the σ values of MCC-650, MCC-750, MCC-850, NSMCC-650, NSMCC-750 and NSMCC-850 were calculated at $897.2 \Omega s^{1/2}$, $1161.3 \Omega s^{1/2}$, $1314.7 \Omega s^{1/2}$, $305.5 \Omega s^{1/2}$, $216.4 \Omega s^{1/2}$ and $448.2 \Omega s^{1/2}$, respectively, indicating that NSMCC materials possessed the more excellent Na^+ transfer than that of MCC materials (Figs. 5b and 5d). Likewise, associated with the analytical results of XPS, it also leads us to consider that the doping dosages of N and S elements would be an important factor to enhance the diffusions of Na^+ because the N and S elements are able to improve the infiltrations of electrolytes and widen the layer spaces of carbon materials.^{21,25,36} In particular, it is distinct that the conductivity of NSMCC-750 is more excellent than other NSMCC materials, causing the NSMCC-750 to possess higher storage capacity than other NSMCC materials. To further unearth the reasons that the NSMCC materials possessed the higher storage capacity than that of MCC materials, the analyses such as CV, dynamics and galvanostatic intermittent titration technique (GITT) measurements were carried out in detail.

As shown in Fig. S7, the reductive peaks attributing to the formations of SEI were observed at 0.8 V of MCC and 1.0 V of NSMCC materials, respectively. Additionally, the reductive peaks around 0.8 V were also observed at the second and third peaks. With respecting to the reports by Zhu et al., these broad peaks are probably ascribed to the defects from the doped N and S elements (Fig. S7).^{21,29}

In accordance with the reports by Wang et al., the dynamics analyses of MCC and NSMCC materials were conducted in detail (Figs. S8 and S9).⁴¹ The capacitive contributions in storage capacity were calculated and illustrated in Table S6. It was clearly found that capacitive contributions to the storage capacity of NSMCC materials are stronger than that of MCC materials. Especially, among the

NSMCC materials, the NSMCC-750 materials manifested a stronger capacitive contribution than other NSMCC materials. Associating with the XPS and EIS results (Figs. 3 and 5a–5d), it is naturally considerable that the contents of doped N and S elements in NSMCC materials are the critical factor to influence the capacitive contribution for storing Na^+ .

In order to more fully confirm the Na^+ ion transfer of MCC and NSMCC materials, the GITT calculations were performed as shown in Figs. S10 and S11. As a result, the accurate calculations reveal that the NSMCC materials exhibited more excellent Na^+ transfer abilities than that of MCC materials in charge and discharge processes (Figs. 5e and 5f). The outstanding Na^+ transfer ability of NSMCC is likely to be related to the doped N and S elements.^{21,29} These aforementioned analyses reveal that the improvement of chemical kinetics by doped N and S elements in NSMCC materials enhances the storage capacity of NSMCC materials.

3.3 The conformations of positive electrode materials of SIHCs

Based on the concept that a positive electrode is usually conformed to the materials possessing the high specific capacity, the electric double layer (EDL) properties of MCC and NSMCC materials were investigated in a potential range of 2.5–4.2 V.

As shown in Fig. 6, it was distinctly observed that all CV curves of MCC and NSMCC materials showed quasi-rectangular shapes without obvious redox peaks, which almost are the ideal capacitive behavior.²⁶ Furthermore, the galvanostatic charge-discharge (GCD) curves were described in Fig. 7. It was found that all of the curves exhibited the characteristic isosceles triangle behaviors, confirming that the storage type of MCC and NSMCC materials mainly were the EDL type. Similar to reports by Huang et al.,⁴² the specific capacities of MCC-650, MCC-750, MCC-850, NSMCC-650, NSMCC-750 and NSMCC-850 were respectively calculated at 87.5 F g^{-1} , 103.7 F g^{-1} , 98.3 F g^{-1} , 98.6 F g^{-1} , 96.0 F g^{-1} and 99.4 F g^{-1} during the current density was set at 0.1 A g^{-1} (Table S7). Meanwhile, when the current density was adjusted to the 5.0 A g^{-1} , the MCC-650, MCC-750, MCC-850, NSMCC-650, NSMCC-750 and NSMCC-850 showed specific capacities at 28.0 F g^{-1} , 78.8 F g^{-1} , 73.6 F g^{-1} , 32.6 F g^{-1} , 68.4 F g^{-1} and 79.4 F g^{-1} , respectively (Table S7).^{43–52} Based on the comparisons, it was funded that MCC-750 possessed the higher capacity at a small current density

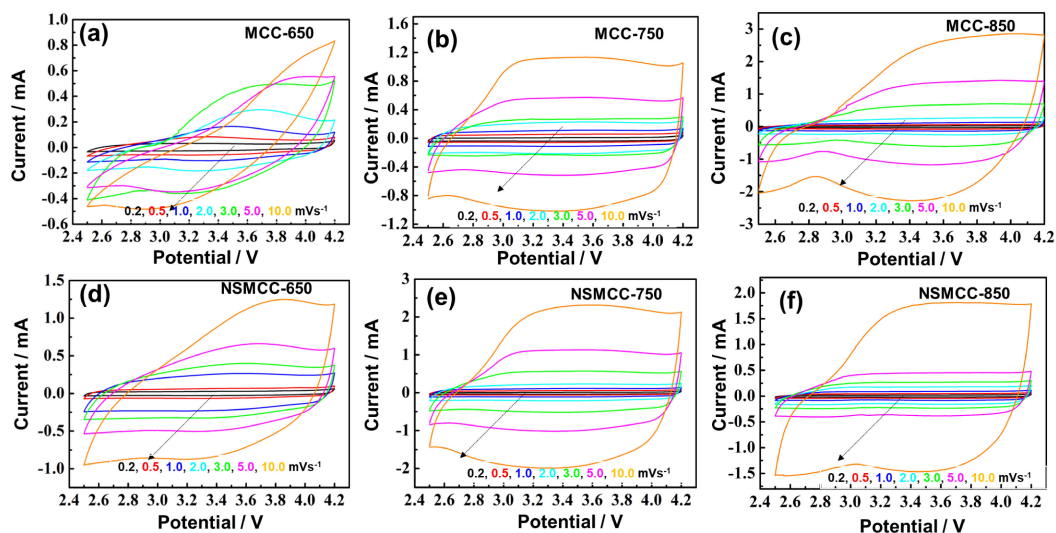


Figure 6. CV curves of MCC materials (a–c) and NSMCC materials (d–f) materials at various scan rates recorded between 2.5–4.2 V.

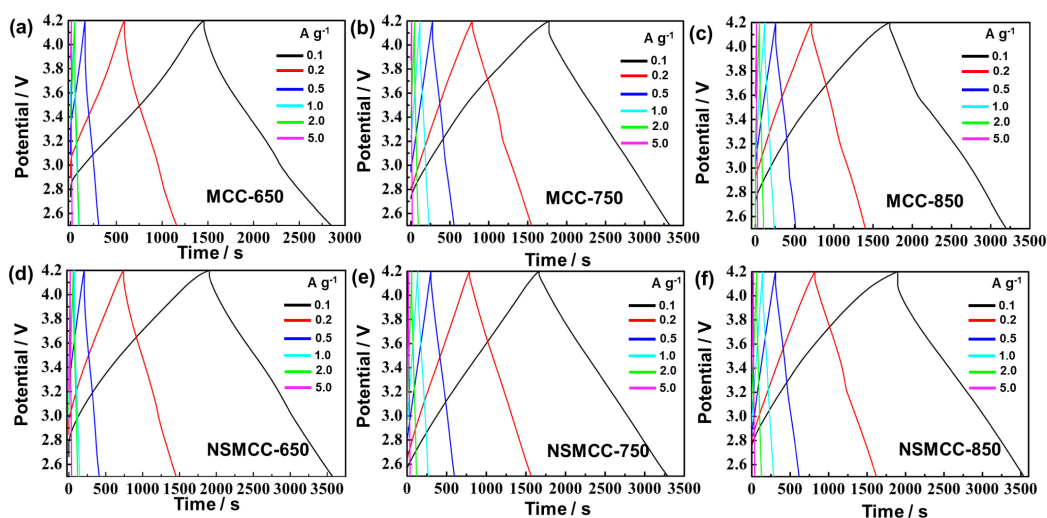


Figure 7. Galvanostatic charge-discharge (GCD) profiles of MCC materials (a–c) and NSMCC materials (d–f) at various current densities.

(0.1 A g^{-1}), and the NSMCC-850 and MCC-750 showed the relatively higher capacity than other materials at a big current density of 5.0 A g^{-1} . Taking both into the considerations of fabrication cost and specific capacity at the same time, the MCC-750 was synthetically decided as a positive electrode of SIHCs.

3.4 The assembly of SIHCs and their electrochemical performance

On the basis of the aforementioned analyses, the NSMCC-750 as a negative electrode and MCC-750 as a positive electrode with different ratios (1 : 1, 1 : 2 and 1 : 3) were used to assemble the SIHCs. As shown in Fig. S12, it was observed that the SIHC(1//1) which was assembled by the NSMCC-750 and MCC-750 (weight ratio of 1 : 1) exhibited a wider operating voltage range than the half-cells assembled by NSMCC-750 and MCC-750, respectively.

After carrying out the CV measurements at different sweeping rates, the CV behaviors of SIHCs which were constructed by MCC and NSMCC materials manifested the rectangular-like behaviors (Fig. S13). Additionally, the GCD behaviors of SIHCs also showed a triangle-like type (Fig. S14). These results suggest that EDL plays the main role to enhance the storage capacity of assembled SIHCs in our studies.

According to the reports by Ajuria et al., the specific capacity of SIHCs which were constructed by NSMCC-750 and MCC-750 in different ratios were calculated at different current densities.²² As shown in Fig. 8a, it was observed that SIHC(1//1) exhibited the higher specific capacity than that of other assembled SIHCs. For example, when the current density was set at 0.1 A g^{-1} , the SIHC(1//1) exhibited the specific capacity at 80.2 F g^{-1} , which was higher than the specific capacity of 52.1 F g^{-1} (SIHC(1//2)) and 48.2 F g^{-1} (SIHC(1//3)), respectively. Additionally, after the current density had been set at 5 A g^{-1} , the above three SIHCs showed the specific capacity at 21.1 F g^{-1} , 18.0 F g^{-1} and 16.5 F g^{-1} , respectively (Table S8). Meanwhile, the SIHC(1//1) exhibited a higher energy density and power density than SIHC(1//2) and (SIHC(1//3)), respectively (Fig. 8b). For instance, the SIHC(1//1) shows an energy density of 100.8 Wh Kg^{-1} at a power density of 136.8 W Kg^{-1} at 0.1 A g^{-1} and a power density of $12957.6 \text{ W Kg}^{-1}$ at an energy density of 46.9 Wh Kg^{-1} at 5 A g^{-1} (Fig. 8b). In addition, the SIHC(1//1) also exhibited more excellent specific capacitance and power density than the SIHCs constructed by other reported materials (Fig. S15, Tables S9 and S10).^{13,25,53–58} Finally, the stabilities at large current densities were described in Fig. 8c. The SIHC(1//1) also showed the capacity retention at 64.5 % over 10000

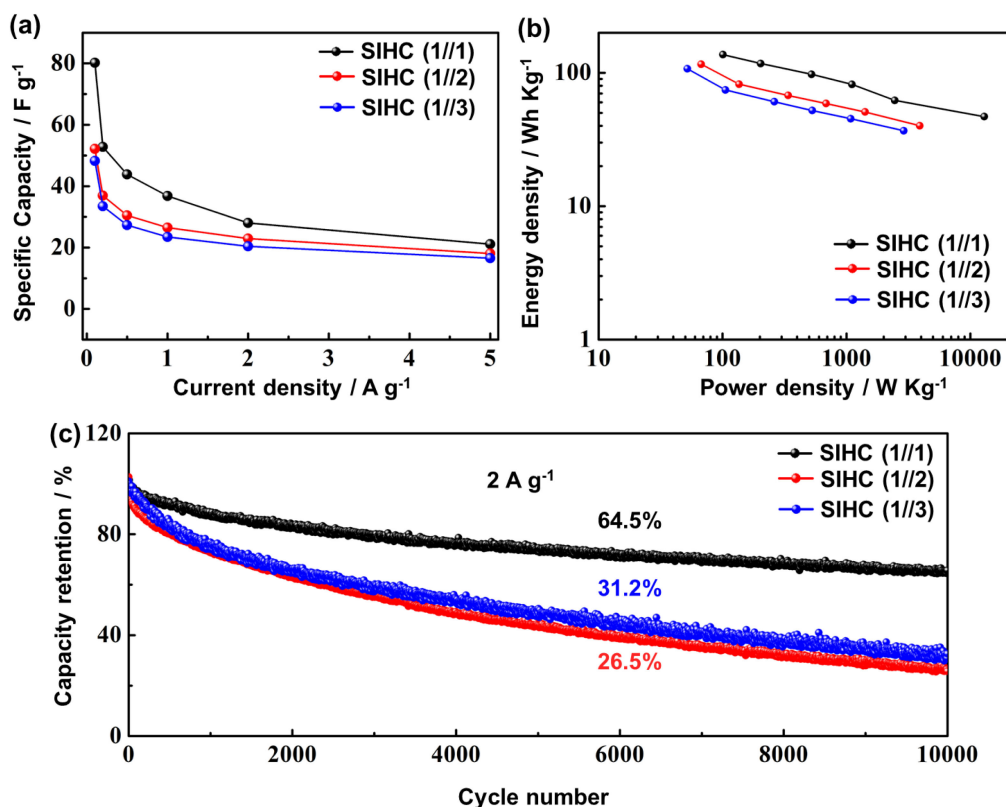


Figure 8. The relationships between specific capacitance and current density of SIHCs (a), and Ragone plots of SIHCs (b). Long-term cycling performance of SIHCs at 2.0 A g⁻¹ (c).

cycles, which was remarkably higher than the SIHC(1//2) and SIHC(1//3). These results indicate that the SIHC(1//1) possesses more impressive electrochemical stability than others.

4. Conclusions

The SIHCs are successfully assembled by carbon electrodes fabricated by using the same carbon source of magnesium citrate. In assembling processes, the materials obtained by direct carbonizations of magnesium citrate are used as positive electrodes, and N-doped and S-doped carbon materials which were obtained by the co-carbonization of magnesium citrate with ammonium persulfate are used as negative electrodes. It is observed that the SIHC(1//1) manifests tremendous electrochemical performance when the weight ratio of positive and negative electrodes was set at 1 : 1. For instance, SIHC(1//1) shows an energy density of 100.8 Wh Kg⁻¹ at a power density of 136.8 W Kg⁻¹ at 0.1 A g⁻¹. Furthermore, this SIHC(1//1) also displays a power density of 12957.6 W Kg⁻¹ at an energy density of 46.9 Wh Kg⁻¹ at 5 A g⁻¹. The aforementioned results indicate that using the one carbon source is able to fabricate the SIHCs having the competitively electrochemical performance. Thus, we consider that our studies can also provide a beneficial reference to facilely fabricate the SIHCs having tremendous electrochemical performance.

Acknowledgments

We are grateful to the support of University of Science and Technology Liaoning (601009816-39) and 2017RC03. This work obtains the support by the Liaoning Province Education Department of China (Grant No. 601009887-16). This work is partly supported with the project supported by the National Natural Science Foundation of China (Grant No. 51672117 and 51672118).

CRediT Authorship Contribution Statement

Jianke Li: Conceptualization (Equal), Data curation (Equal), Formal analysis (Equal), Writing – original draft (Equal)
 Wenjie Liang: Conceptualization (Equal), Data curation (Equal), Formal analysis (Equal), Investigation (Equal)
 Xincheng Miao: Methodology (Lead), Supervision (Lead), Writing – review & editing (Equal)
 Beibei Han: Formal analysis (Equal), Investigation (Equal), Methodology (Supporting)
 Guiying Xu: Conceptualization (Equal), Investigation (Equal), Methodology (Equal), Writing – original draft (Supporting)
 Kun Wang: Data curation (Equal), Formal analysis (Equal), Investigation (Equal), Methodology (Equal), Writing – review & editing (Supporting)
 Baigang An: Project administration (Lead), Supervision (Equal)
 Dongying Ju: Project administration (Equal), Resources (Equal), Supervision (Equal)
 Maorong Chai: Methodology (Equal), Project administration (Equal), Supervision (Equal)
 Weimin Zhou: Conceptualization (Lead), Resources (Lead), Writing – review & editing (Lead)

Data Availability Statement

The data that support the findings of this study are openly available under the terms of the designated Creative Commons License in J-STAGE Data listed in D1 of References.

Conflict of Interest

The authors declare no conflict of interest in the manuscript.

Funding

University of Science and Technology Liaoning: 601009816-39
 University of Science and Technology Liaoning: 2017RC03
 Liaoning Province Education Department of China : 601009887-16
 National Natural Science Foundation of China: 51672117
 National Natural Science Foundation of China: 51672118

References

- D1. J. Li, W. Liang, X. Miao, B. Han, G. Xu, K. Wang, B. An, D. Ju, M. Chai, and W. Zhou, *J-STAGE Data*, <https://doi.org/10.50892/data.electrochemistry.22631050>, (2023).
1. Y. Li, M. Chen, B. Liu, Y. Zhang, X. Liang, and X. Xia, *Adv. Energy Mater.*, **10**, 2000927 (2020).
 2. Z. Liu, X. Zhang, D. Huang, B. Gao, C. Ni, L. Wang, Y. Ren, J. Wang, H. Gou, and G. Wang, *Chem. Eng. J.*, **379**, 122418 (2020).
 3. X. Yang and A. L. Rogach, *Adv. Energy Mater.*, **10**, 2000288 (2020).
 4. L. Zhu, Y. Li, J. Wang, and X. Zhu, *Solid State Ionics*, **327**, 129 (2018).
 5. W. Hao, H. Si, W. Li, C. Zhang, W. Zhu, and X. Qiu, *Solid State Ionics*, **343**, 115071 (2019).
 6. Y. Xiao, S. H. Lee, and Y.-K. Sun, *Adv. Energy Mater.*, **7**, 1601329 (2017).
 7. Z. Hu, L. X. Wang, K. Zhang, J. Wang, F. Cheng, Z. Tao, and J. Chen, *Angew. Chem.*, **53**, 12794 (2014).
 8. B. Wang, X. Gao, L. Xu, K. Zou, P. Cai, X. Deng, L. Yang, H. Hou, G. Zou, and X. Ji, *Batteries Supercaps*, **4**, 538 (2021).
 9. R. Yan, E. Josef, H. Huang, K. Leus, M. Niederberger, J. P. Hofmann, R. Walczak, M. Antonietti, and M. Oschatz, *Adv. Funct. Mater.*, **29**, 1902858 (2019).
 10. X. Zhao, Y. Zhao, Z. Liu, Y. Yang, J. Sui, H.-E. Wang, W. Cai, and G. Cao, *Chem. Eng. J.*, **354**, 1164 (2018).
 11. F. Li and Z. Zhou, *Small*, **14**, 1702961 (2018).
 12. X. Zhao, Y. Zhang, Y. Wang, and H. Wei, *Batteries Supercaps*, **2**, 899 (2019).
 13. Z. Le, F. Liu, P. Nie, X. Li, X. Liu, Z. Bian, G. Chen, H. B. Wu, and Y. Lu, *ACS Nano*, **11**, 2952 (2017).
 14. S. Y. Cho, H. J. Yoon, N. R. Kim, Y. S. Yun, and H.-J. Jin, *J. Power Sources*, **329**, 536 (2016).
 15. G. Dong, H. Wang, W. Liu, J. Shi, S. Sun, D. Li, H. Zhang, Y. Yang, and Y. Cui, *ACS Appl. Energy Mater.*, **1**, 5636 (2018).
 16. L. Gao, G. Chen, L. Zhang, B. Yan, and X. Yang, *Electrochim. Acta*, **379**, 138185 (2021).
 17. B. Yang, J. Chen, S. Lei, R. Guo, H. Li, S. Shi, and X. Yan, *Adv. Energy Mater.*, **8**, 1702409 (2018).
 18. L.-F. Que, F.-D. Yu, X.-L. Sui, L. Zhao, J.-G. Zhou, D.-M. Gu, and Z.-B. Wang, *Nano Energy*, **59**, 17 (2019).
 19. J. Niu, J. Guan, M. Dou, Z. Zhang, J. Kong, and F. Wang, *ACS Appl. Energy Mater.*, **3**, 2478 (2020).
 20. J. Ding, H. Wang, Z. Li, K. Cui, D. Karpuzov, X. Tan, A. Kohandehghan, and D. Mitlin, *Energy Environ. Sci.*, **8**, 941 (2015).
 21. S. Zhu, X. Dong, H. Huang, and M. Qi, *J. Power Sources*, **459**, 228104 (2020).
 22. J. Ajuria, E. Redondo, M. Armaiz, R. Mysyk, T. Rojo, and E. Goikolea, *J. Power Sources*, **359**, 17 (2017).
 23. K. Kuratani, M. Yao, H. Senoh, N. Takeichi, T. Sakai, and T. Kiyobayashi, *Electrochim. Acta*, **76**, 320 (2012).
 24. R. Thangavel, B. K. Ganesan, V. Thangavel, W.-S. Yoon, and Y.-S. Lee, *ACS Appl. Energy Mater.*, **4**, 13376 (2021).
 25. J. Xu, Z. Liu, F. Zhang, J. Tao, L. Shen, and X. Zhang, *RSC Adv.*, **10**, 7780 (2020).
 26. S. Chen, Q. Kuang, and H. J. Fan, *Small*, **16**, 2002803 (2020).
 27. R. Fei, H. Wang, Q. Wang, R. Qiu, S. Tang, R. Wang, B. He, Y. Gong, and H. Fan, *Adv. Energy Mater.*, **10**, 2002741 (2020).
 28. L. Han, Z. Wang, D. Kong, L. Yang, Z. Wang, and F. Pan, *J. Mater. Chem. A*, **6**, 21280 (2018).
 29. R. Wu, S. Chen, J. Deng, X. Huang, Y. Song, R. Gan, X. Wang, and Z. Wei, *J. Energy Chem.*, **27**, 1661 (2018).
 30. T. Morishita, Y. Soneda, T. Tsumura, and M. Inagaki, *Carbon*, **44**, 2360 (2006).
 31. M.-S. Chen, W. Fu, Y. Hu, M.-Y. Chen, Y.-J. Chiou, H.-M. Lin, M. Zhang, and Z. Shen, *Nanoscale*, **12**, 16262 (2020).
 32. S. A. A. Mansour, *Thermochim. Acta*, **233**, 231 (1994).
 33. J. Ding, H. Wang, Z. Li, K. Cui, D. Karpuzov, X. Tan, A. Kohandehghan, and D. Mitlin, *Energy Environ. Sci.*, **8**, 941 (2015).
 34. Z. Liu, X. Zhang, D. Huang, B. Gao, C. Ni, L. Wang, Y. Ren, J. Wang, H. Gou, and G. Wang, *Chem. Eng. J.*, **379**, 122418 (2020).
 35. H. Gao, W. Ma, W. Yang, J. Wang, J. Niu, F. Luo, Z. Peng, and Z. Zhang, *J. Power Sources*, **379**, 1 (2018).
 36. R. Yin, K. Wang, B. Han, G. Xu, L. Li, B. An, D. Ju, M. Chai, S. Li, and W. Zhou, *Coatings*, **11**, 948 (2021).
 37. Y. Liu, J. S. Xue, T. Zhang, and J. R. Dahn, *Carbon*, **34**, 193 (1996).
 38. W. Luo, Z. Jian, Z. Xing, W. Wang, C. Bommier, M. M. Lerner, and X. Ji, *ACS Cent. Sci.*, **1**, 516 (2015).
 39. J. Zhu, Y. Xu, Y. Zhang, T. Feng, J. Wang, S. Mao, and L. Xiong, *Carbon*, **107**, 638 (2016).
 40. X. Wang, S. He, F. Chem, and X. Hou, *Energy Fuels*, **34**, 13144 (2020).
 41. K. Wang, D. Y. Ju, G. Y. Xu, B. B. Han, M. R. Chai, Y. F. Wang, L. X. Li, X. H. Zhang, M. Ucida, and W. M. Zhou, *Sci. China Technol. Sci.*, **63**, 2709 (2020).
 42. T. Huang, X. Chu, S. Cai, Q. Yang, H. Chen, Y. Liu, K. Gopalsamy, Z. Xu, W. Gao, and C. Gao, *Energy Storage Mater.*, **17**, 349 (2019).
 43. J. Zhu, J. Roscowc, S. Chandrasekaran, L. Deng, P. Zhang, T. He, K. Wang, and L. Huang, *ChemSusChem*, **13**, 1275 (2020).
 44. K. Zou, P. Cai, C. Liu, J. Li, X. Gao, L. Xu, G. Zou, H. Hou, Z. Liu, and X. Ji, *J. Mater. Chem. A*, **7**, 13540 (2019).
 45. Y.-E. Zhu, L. Yang, J. Sheng, Y. Chen, H. Gu, J. Wei, and Z. Zhou, *Adv. Energy Mater.*, **7**, 1701222 (2017).
 46. X. Wang, S. Kajiyama, H. Inuma, E. Hosono, S. Oro, I. Moriguchi, M. Okubo, and A. Yamada, *Nat. Commun.*, **6**, 6544 (2015).
 47. B. Yang, J. Chen, S. Lei, R. Guo, H. Li, S. Shi, and X. Yan, *Adv. Energy Mater.*, **8**, 1702409 (2018).
 48. J. Zhang, W. Lv, D. Zheng, Q. Liang, D.-W. Wang, F. Kang, and Q.-H. Yang, *Adv. Energy Mater.*, **8**, 1702395 (2018).
 49. W. Yang, W. Yang, F. Ding, L. Sang, Z. Ma, and G. Shao, *Carbon*, **111**, 419 (2017).
 50. H. Li, Y. Zhu, S. Dong, L. Shen, Z. Chen, X. Zhang, and G. Yu, *Chem. Mater.*, **28**, 5753 (2016).
 51. D. Zhao, X. Wu, and C. Guo, *Inorg. Chem. Front.*, **5**, 1378 (2018).
 52. H. Wang, C. Zhu, D. Chao, Q. Yan, and H. Fan, *Adv. Mater.*, **29**, 1702093 (2017).
 53. G. Subburam, K. Ramachandran, S. A. El-Khodary, B. Zou, J. Wang, L. Wang, J. Qiu, X. Liu, D. H. L. Ng, and J. Lian, *Chem. Eng. J.*, **415**, 129012 (2021).
 54. D. Li, C. Ye, X. Chen, S. Wang, and H. Wang, *J. Power Sources*, **382**, 116 (2018).
 55. F. Yu, Z. Liu, R. Zhou, D. Tan, H. Wang, and F. Wang, *Mater. Horiz.*, **5**, 529 (2018).
 56. Q. Zhao, D. Yang, C. Zhang, X.-H. Liu, X. Fan, A. K. Whittaker, and X. S. Zhao, *ACS Appl. Mater. Interfaces*, **10**, 43730 (2018).
 57. Z. Chen, V. Augustyn, X. Jia, Q. Xiao, B. Dunn, and Y. Lu, *ACS Nano*, **6**, 4319 (2012).
 58. Q. Zhao, D. Yang, A. K. Whittaker, and X. S. Zhao, *J. Power Sources*, **396**, 12 (2018).